Biomedical Microdevices (2021) 23: 12
https://doi.org/10.1007/s10544-021-00553-4

Rapid fabrication of teflon apertures by controlled high voltage pulses for formation of free standing planar lipid bilayer membrane

Yasin Ozturk[1] · Aliakbar Ebrahimi[2] · Araz Norouz Dizaji[2] · Ozge Kaygusuz[3] · Jayesh Arun Bafna[4] · Mathias Winterhalter[4] · Guven Cankaya[1] · Cihan Darcan[3,5] · Fatma Dogan Guzel[2]

Accepted: 16 February 2021 / Published online: 27 February 2021

Abstract

Free standing artificial lipid bilayers are widely used in the study of biological pores. In these types of studies, the free standing planar lipid bilayer is formed over a micron-sized aperture consisting of either polymer such as Polytetrafluoroethylene (PTFE, Teflon) or glass. Teflon is chemically inert, has a low dielectric constant, and has a high electrical resistance which combined allow for obtaining low noise recordings. This study investigates the reproducible generation of micropores in the range of 50–100 microns in diameter in a Teflon film using a high energy discharge set-up. The discharger set-up consists of a microprocessor, a transformer, a voltage regulator, and is controlled by a computer. We compared two approaches for pore creation: single and multi-pulse methods. The results showed that the multi-pulse method produced narrower aperture size distributions and is more convenient for lipid bilayer formation, and thus would have a higher success rate than the single-pulse method. The bilayer stability experiments showed that the lipid bilayer lasts for more than 33 h. Finally, as a proof-of-concept, we show that the single and multi-channel electrophysiology experiments were successfully performed with the apertures created by using the mentioned discharger. In conclusion, the described discharger provides reproducible Teflon-pores in a cheap and easy-to-operate manner.

Keywords PTFE · Micromachining · Micropore · High voltage transformer · Lipid bilayer · Single channel electrophysiology · OmpF porin

1 Introduction

Electrophysiology is the main method of choice to studying the electrochemical properties of biological cells and tissues (patch-clamping). Due to its sensitivity, this approach became the basis of single-molecule detection (nanopore studies) (Scanziani and Häusser 2009; Molleman and Patch clamping, 2003; Miles et al. 2013; Güzel and Miles 2018; Guzel and Avci 2018). The underlying principle is to apply an ionic current across the biological or artificial membrane of interest containing a water-filled protein channel (Benz et al. 1978; Montal and Mueller 1972; Mueller et al. 1962; Schmidt et al. 2000; Gornall et al. 2011; Hagge et al. 2002). Minor changes in the conductance, caused for example by insertion or a conformational change of a protein, can then be detected exclusively. Due to the contrast in conductance, electrophysiology is the most suitable technique for detecting small changes in membrane conductance. Recording the ion current across the membrane proteins provides vast information about channel structure, ion selectivity, changes in channel conformation, and possibly the passage of uncharged molecules (Hagge et al. 2004; Dilger and Benz 1985; Bähr et al. 1998). Membrane proteins are inserted into a free standing lipid bilayers formed across a solid-state micron-sized aperture (Zhang 2012; Obergrussberger et al. 2015; Brown et al. 2008; Priest et al. 2007; Siontorou et al. 2017). The supporting material to form the lipid bilayer may

✉ Fatma Dogan Guzel
fdogan@ybu.edu.tr

[1] Department of Metallurgical and Materials Engineering, Ankara Yıldırım Beyazıt University, Ankara, Turkey

[2] Department of Biomedical Engineering, Ankara Yıldırım Beyazıt University, Ankara, Turkey

[3] Biotechnology Application and Research Center, Bilecik Seyh Edebali University, Bilecik, Turkey

[4] Department of Life Sciences and Chemistry, Jacobs University Bremen, Bremen, Germany

[5] Department of Molecular Biology and Genetics, Bilecik Seyh Edebali University, Bilecik, Turkey

vary from glass to polymer (Harroun et al. (1999); Charitat et al. 1999). Materials with low dielectric constants (< 3) and high electrical resistance such as Polytetrafluoroethylene (PTFE), Polypropylene (PP), and Polymethyl methacrylate (PMMA) have been studied in low noise electrophysiology recordings and the aperture to form the lipid bilayer on it can be melted or burned by methods such as SACE (Spark Assisted Chemical Engraving), indentation, laser ablation, etc. (Maex et al. 2003; Sandison et al. 2007; Mayer et al. 2003; Hansen et al. 2009). These methods require special equipment such as wet electrolyte set-ups, special tip types, or thin-film technologies to generate micropores while advantageously working for all the above-mentioned dielectric materials. SACE serves micro-milling technology by using both the electrolytic environment and thermal manipulation with the help of a high voltage spark generator. Commercially available high-frequency spark generators used to create micropores on PTFE (Teflon) are currently very expensive (Hanke and Schulue 2012), despite the reports that some parts (i.e. ignition coil) were used in search for cheaper methods (Holst and ed., 2000). In contrast, more accessible techniques such as push-button techniques have become appreciated for their use recently (Bandara et al. 2019). There seem to be pros and cons for each technique in terms of their availability, price, and ease of utilization.

In this study, we present the development of a time-modulated, easy-to-operate, controllable and inexpensive high voltage discharge technique to create a micron-sized aperture on Teflon and demonstrate its application in low-noise electrophysiological recordings. The paper herein describes the step-by-step setting of the discharger and its electrical connections. We believe that the setting of the high voltage discharger will facilitate septum preparation in an easy and reproducible manner.

2 Materials and methods

2.1 High voltage discharge settings

The high voltage discharge setting includes mainly six components: Arc ignition platform, transformer, voltage regulator, microprocessor, power supply and a computer. The schematic of the arc ignition platform and component connections are shown in Fig. 1a and Fig. 1b, respectively. The arc ignition platform consists of a base, two electrodes, and a glass film holder. The base is made of Polyoxymethylene (POM) and provides a setting for electrode movement while also holding the glass film holder in-between the two electrodes. Electrodes are made of nickel-coated copper with an ending of rounded spring-loaded pins (pogo pins). The gap in-between the two electrodes was adjusted through the moveable POM platform (See Supplementary Fig. 1). All experiments were carried out with a 1 mm gap between each electrode and the film holder. 3 cm × 3 cm wide and 25 µm thick Teflon film (Goodfellow, UK) was sandwiched between two modified glass slides with an aperture size of 1.5 cm. The arc discharge was sparked over a film region that covers the aperture. The joints and cables that connect the electrodes to the transformer were insulated with silicone rubber against corona leakage for a stable output voltage of approximately 20 kV.

A step-up dual primary winding type transformer was made in-house since it can be easily transformed into DC output by changing the electrical inputs and the voltage regulation parts. Windings made of insulated copper were constructed on a machined Teflon rod such that the number of turns required for the secondary winding was appropriate. The primary winding contains four pins (two main and two feedback pins) in order to assist the alternating current flow between the electrodes. The total number of secondary winding coils with an outer diameter of 0.1 mm was 3380 (See Supplementary Fig. 2).

The transformer was connected to a bipolar junction NPN type transistor via the primary winding. The transistor was then used to amplify the voltage up to 100 V. The transistor provides a stable AC frequency of 50 Hz to the primary coil by utilizing the main and the feedback pins of the primary windings. This leads to a serial magnetic field change, and thus alternating current flow occurs on the secondary coil as desired. The transistor acts as a voltage regulator and was connected to a conventional microprocessor (Arduino Nano, Italy) for the adjustment of spark discharge time between the electrodes. The microprocessor triggers an electro-mechanic relay (Omron, Japan) in order to enable current flow without

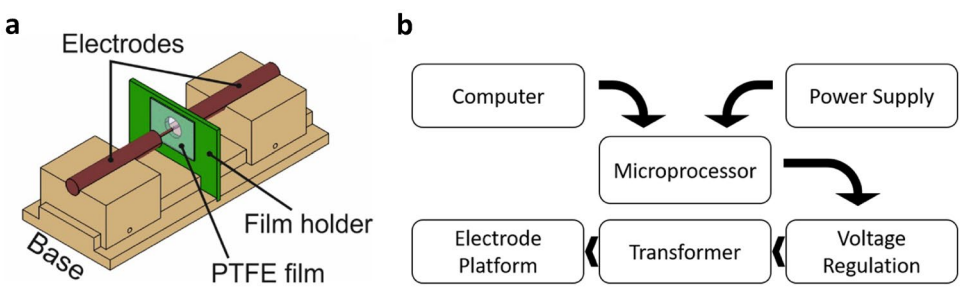

Fig. 1 Schematics of the setting. **a** Schematic representation of the arc ignition platform used in the high voltage discharger setting. **b** Schematic of the working mechanism of high voltage discharger

harming the microprocessor. The power supply was used to provide 9 V of potential while the computer was employed to control and monitor the time settings.

2.2 Optical and SEM characterizations

After aperture opening, the Teflon was gently removed, examined using an optical microscope (inverted, Euromex Oxion Inverso), and the hole diameter was calculated using the microscope software (Image Focus 4). Scanning Electron Microscope (SEM, Hitachi SU5000, Japan) was performed at a magnification of 1000X with 30° tilting.

2.3 Bilayer formation

Planar lipid bilayers were formed according to the monolayer technique of Montal and Mueller (Montal and Mueller 1972; Gutsmann et al. 2015). Experiments were carried out using a cuvette made of Teflon. The Teflon film possessing the micron size aperture was sandwiched between the two cells (cis and trans) of the cuvette. A pore of 100 µm in diameter was opened up on a 25 µm Teflon film using the above-mentioned discharger. The cuvettes were placed on a Teflon base to reduce vibration, in order to reliably form the lipid layer during the experiment and to ensure stability during the experiments (See Supplementary Fig. 3). Each cuvette chamber is capable of containing approximately 3 mL of liquid. The surface of the Teflon aperture was painted on both sides with approximately 3 µL of 95% hexane (Merck, DE) solution containing 1% hexadecane and was left for 15 min for the hexane to evaporate. Thus, a hydrophobic layer was formed around the aperture. The cuvette cells were then filled with 1 M KCl, 10 mM HEPES (pH 7,5) and placed in a Faraday box. Electrical recordings were made through a pair of Ag/AgCl electrodes (World Precision Instruments, Sarasota, FL), attached to an Axon Instruments 200B amplifier with a capacitive head-stage, digitized by an Axon Digidata 1550B digitizer, computer-controlled by Clampex 10.0 (all by Axon Instruments, Foster City, CA). The data was filtered by an analog low-pass four-pole Bessel filter at 5 kHz and digitally sampled at 100 kHz. Data analysis was conducted with Clampfit 10.0. The two electrodes were immersed into the cuvettes: the electrode on the cis side of the cell was grounded, whereas the electrode on the trans side was connected to the head-stage. The amplifier measures the current passing through the aperture in the film while forming the lipid bilayer and during the single-channel experiments. The Faraday cage and the amplifier were grounded to reduce electrical noise. First, the current flowing through the pore in the film was measured at the amplifier ($I_{aperture}$ > 20 nA) and when the aperture was found to be open, 3 µl of 5 mg/mL 1,2-diphytanoyl-sn-glycero-3-phosphocholine (DPhPC) (Avanti Polar Lipids, USA) dissolved in 1 mL 95% n-Pentane (Merck, DE) was added to each chamber. Using 5 mL micro-pipettes, the solution was pipetted up and down and the current was recorded in the amplifier. When the current value decreased to 0 pA, this was an indication that the lipid bilayer was formed around the aperture with gigaohm-seal. Afterward, single-channel experiments were performed: 1 µl of 3×10^{-5} mg/ml purified detergent-solubilized OmpF porin solution was added to the cis chamber and voltages of different ranges (25, 50, 75, 100, 150 and 200 mV) were applied while mixing the chamber gently for porin insertion into the lipid bilayer membrane.

2.4 Cloning, expression, and purification of *E. coli* OmpF porin protein

Primers of the OmpF gene (pLATE51 OmpF forward primer: 5′ GGTGATGATGATGACAAGATGCTAAAA GCACAAAAACTTA 3′, pLATE51 OmpF reverse primer: 5′ GGAGATGGGAAGTCATTAGAATAATTT CACAGGAATATCT 3′) were designed in accordance with the pLATE51 vector in the aLICator LIC Cloning and Expression Kit 2 (ThermoFisher Scientifics K1251). The PCR product of the *E. coli* ompF porin gene which was amplified by colony PCR using specific primers (plasmid primers; Forward 5′- TAATACGACTCACTA TAGGG -3′, Reverse 5′- GAGCGGATAACAATTTCA CACAGG-3) was cloned into the pLATE51 vector. The plasmid was then transformed into a wild-type *E. coli* W3110 strain. Transformant *E. coli* was then transferred to 100 ml LB broth, incubated at 160 rpm at 37 °C until the OD_{600} value reached 0.6–0.8 absorbance. After that, a final concentration of 0.5 mM IPTG was added to the culture and 6 h of shaking incubation was continued to induce the plasmid. After incubation, 100 ml bacterial cells (approximately 1.1×10^{11} number of cells) were centrifuged at 12,000 rpm for 5 min at 4 °C. The next processes were carried out according to the purification procedure of Protino Ni–NTA His-tag proteins. 5 ml of NPI-10 (50 mM NaH_2PO_4, 300 mM NaCl, 10 mM imidazole pH 8.0) buffer was added onto the collected 1 g cell pellet and the pellet was dissolved in this buffer. Later, lysozyme was added to this cell suspension at a final concentration of 1 mg / ml and lysed on ice for 30 min. Then the cells were sonicated. After sonication, the suspension was centrifuged at 10,000 g for 30 min at 4 °C and the supernatant was discarded, and the pellet (inclusion bodies) was kept on ice. The pellet was then washed by adding 10 mL of NPI-10 buffer onto the pellet. It was centrifuged again at 10,000 g for 30 min at 4 °C and the supernatant was discarded. 2.0 mL of DNPI-10

(50 mM NaH_2PO_4, 300 mM NaCl, 10 mM imidazole, 8.0 M urea, pH 8.0) buffer was added onto the obtained pellet and the pellet was dissolved. The suspension was then centrifuged at 10,000 g for 30 min at 20 °C to remove insoluble materials. The supernatant was then transferred to a clean tube. The Ni–NTA was equilibrated by washing with agarose buffer (0.5 M NaOH for 30 min) and then mixed with the balanced agarose protein supernatant and left to incubate at 9 rpm for 1–4 h at 4 °C shaking. After the incubation, the supernatant was centrifuged at 4000 rpm for 1 min at 4 °C. After centrifugation, the supernatant was transferred to a clean flask and stored at -20 °C. 800 µl of DNPI-20 (50 mM NaH_2PO_4, 300 mM NaCl, 20 mM imidazole, 8 M urea pH 8.0) buffer was then added onto the pellet and the pellet was washed with this buffer. It was then centrifuged at 4000 rpm for 1 min at 4 °C. This process is repeated 3 times. After the last washing process, DNPI-250 (50 mM NaH_2PO_4, 300 mM NaCl, 250 mM imidazole, 8 M urea pH 8.0) buffer was added onto the pellet and centrifuged at 4000 rpm for 1 min at 4 °C. This process was repeated 3 times. Purified proteins were analyzed by western blot using anti-histag antibody (Mahmood and Yang 2012; Zhu et al. 2013; Wang et al. 2017; Gabe et al. 2017). Then, cutting with a tev protease (cat. No. E027) was performed to remove the histidine tail from the protein. Imidazole and urea from the targeted protein were removed using a dialysis membrane. All samples obtained were stored at -80 °C. Porins were then diluted to a concentration of 1% using n-octylpolyoxyethylene solution for the single-channel experiments and stored at 4 °C for short term use.

3 Results and discussion

3.1 Instrument settings

The components and parameters of the discharger were carefully chosen in order to obtain well-defined micro-sized round apertures. Rounded tip pogo pins were chosen because their use would decrease the corona effect while blocking untimely triggering and decreasing unwanted surface abnormalities on micropores (Altamimi et al. 2014). In addition, we observed that the electrode gap was key in establishing controlled ignition; if the electrode gap was increased, the air space and insulating Teflon would make arc transmission difficult. Preliminary experiments were carried out with a 7 mm electrode gap; however, the aperture diameter could not be controlled stably as the arc transmission became difficult. We believe that the arc transmission that was unpredictably formed between the opposite electrodes in these experiments, which we believe it accelerates although it was already high during melting. Moreover, increasing the air space between the two electrodes required much more air breakdown voltage, and therefore the experiments were more influenced by the factors such as humidity and instantaneous temperature change of the arc environment (Stokes and Oppenlander 1991; SiamratPhonkaphon 2016). Upon the observation of unpredictable spark ignition, the electrode gap was reduced to 2 mm in between the two electrodes, and this was found to be optimal for the following experiments.

Another consideration taken into account was the trigger time. The spark ignition of the discharger relies on the capacity of the relay and the trigger time. During the initial trials, we found that the spark ignition was obtained within a minimum of 6 ms triggering time. Considering the trigger time and the unpredictability in the formation of the well-defined pore sizes, two different approaches for a successful spark ignition were studied; single-pulse and multi-pulse (time-modulated). 50 ms of single exposure was used for single-pulse experiments whereas serial on-time and off-time pulses for 6 ms and 300 ms, respectively, were applied for multi-pulse ignition. This is illustrated in Fig. 2a, b, respectively.

In single-pulse experiments, 50 ms single exposure was sufficient to form micron-sized pores. In this way, 50 µm or large pore sizes were obtained, even reaching about 400 µm wide-pore sizes in some cases, as shown in Fig. 2c. We assumed that the wide-size distribution was caused by the constant uncontrollable heating and melting of the film.

It was obvious that the single-pulse experiments only produced large pores with low predictability. The necessity of a control mechanism emerged to obtain small pores in a controllable manner. An additional module; PWM (pulse width modulation) before the voltage regulation section was therefore implemented, aiming to introduce high frequency-controlled on and off exposures (to adjust the intensity of the transferred arc). However, an additional module caused more unpredictable results for single-pulse experiments. The PWM module was then discarded for simplicity and pulse modulation was designed. The purpose of this was to ensure the discharge of the high voltage that occurs instantaneously in a short time and to melt the film successfully. The shortest possible on-time pulse was kept at 6 ms, as stated earlier. The off-time pulses lasted for 300 ms. The repeated cycle of on and off-time intervals within about 1 min duration indeed produced the best yield with a narrower pore size distribution. An average of 60 ± 15 µm wide pores were possible to create with this approach.

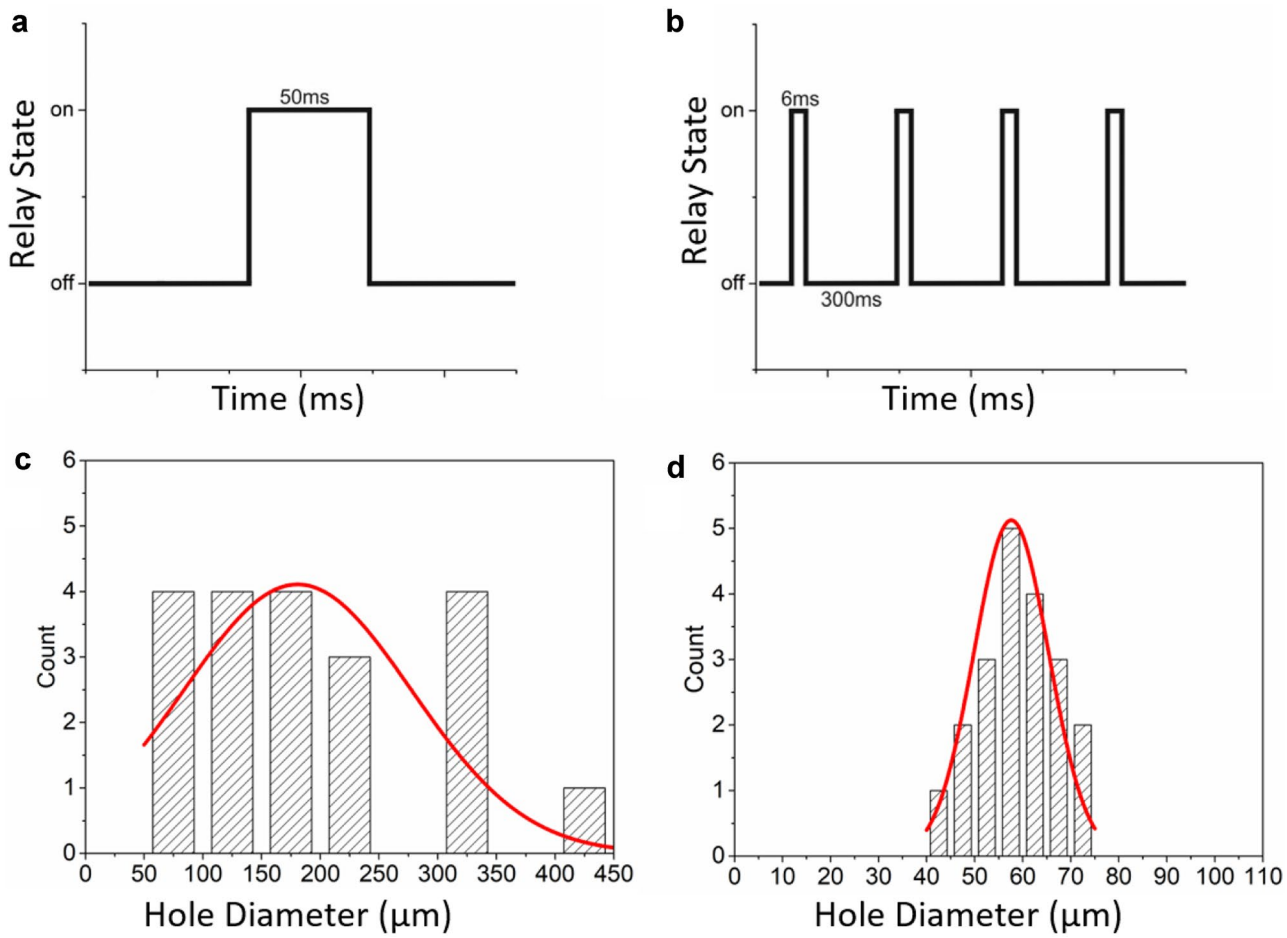

Fig. 2 Arc discharge-time graphs and size-distribution histograms. **a** Single-pulse discharge-time graph. **b** Multi-pulse discharge-time graph. **c** Size distribution histogram of the single-pulse method. **d** Size distribution histogram of the pulse method. The fitting lines in **c** and **d** represent normal distribution fits

3.2 Micropore formation

In the technique described here, micropores form upon the application of the arc discharge due to the melting of the material during the exposure. An optical and an SEM image of the pore created via the multi-pulse approach are shown in Fig. 3a, b respectively. The morphology of the pore seems to be uniformly smooth at the edges throughout the entire aperture.

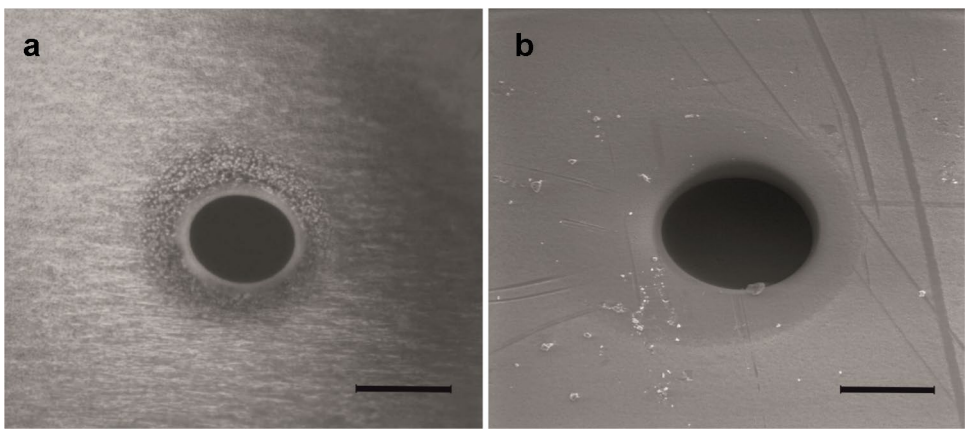

Fig. 3 **a** An optical image of a 54 μm wide aperture. **b** A tilted view of SEM micrograph of an 84 μm sized aperture made by multi-pulse arc discharge. Scale bars are 50 μm

3.3 Lipid bilayer experiments

3.3.1 Bilayer characterization

Initial experiments were performed at a 7 mm electrode distance using single-pulse approach. These resulted in unpredictable lipid bilayer formation and therefore the success rate was considerably low. We presume that this is because of the fact that the distribution of the aperture diameter size was wide and the selection of a particular aperture size among the produced ones was difficult. The success rate of lipid bilayer formation was increased when the multi-pulse method was used; this is a consequence of the narrower aperture size distribution. The success rate for the former was around 30% while the latter was 95% (N:20 experiments). We found that the lipid bilayers formed using the high voltage discharger were relatively stable and do not break when a slight movement occurs around the set-up, unlike similar classical lipid bilayer experiments. Stability experiments were carried out using a Teflon film with a 70 µm sized aperture. We observed that the lipid bilayers were stable for more than 33 h at 0 V and for more than 20 h at 200 mV. After 33 h, we purposely broke the lipid bilayers by applying successive high voltages (HV) (1 V for 50 ms, successive zapping). High voltage response and resealing characteristics of the bilayer can be seen in Fig. 4. The resealing of the membrane may be due to the fact that the pore formation was not large enough to disrupt the membrane because insufficient bubble formation may occur on the membrane when HV was applied (Wrenn et al. 2013; Winterhalter 2014). The mechanical rupture (membrane disruption) was observed after the 5th application of HV. This result is consistent with observations in previous studies (Wonderlin et al. 1990; Eray et al. 1994). To the best of our knowledge, lipid bilayers formed using film apertures opened via different instruments and/or set-ups such as high-frequency generators and spark discharge methods tend to break and/or leak when higher than around 300 mV was applied (Mayer et al. 2003; Hanke and Schulue 2012; Winterhalter 2014). Our discharger also produced similar results to the lipid bilayer formation experiments performed using glass capillaries where the stability is claimed to be higher (Guzel and Citak 2018).

Noise performance is another consideration to take into account in similar studies (Mayer et al. 2003; Maglia et al. 2010; Wilk et al. 2007). For comparison to the literature, we investigated the root mean square (RMS) noise while monitoring the signals of formed bilayers. An aperture with a diameter of 90 µm made by a commercially available high frequency-spark generator produced an RMS value of 2.43 ± 0.05 pA while the RMS value for an aperture of 70 µm created by our discharger was 1.93 ± 0.01 pA under the same conditions. These results are reasonably similar to the published studies and theoretical approximations (Mayer et al. 2003; Peterman et al. 2002). The slight difference is a consequence of the difference in the aperture sizes.

3.3.2 Channel recordings

Single-channel experiments were carried out using OmpF diffusion channel of *E. coli*. It was selected due to known literature and its easy insertion into the bilayer (Guzel and Citak 2018). Once a stable lipid bilayer was formed, the diluted porin solution was added to the cis cell of the cuvette. Both multichannel and single-channel OmpF porin insertions were observed upon the application of 150 mV or higher depending on the concentration of the dilution. For example, Fig. 5a shows three successive trimeric OmpF insertion (after addition of 3 µl of 300 pM OmpF stock solution into 3 ml 0.2 M KCl solution and 200 mV transmembrane voltage). Each step corresponds to about 200 pA in the current recorded at 200 mV indicating the insertion of one trimer. Figure 5b shows the

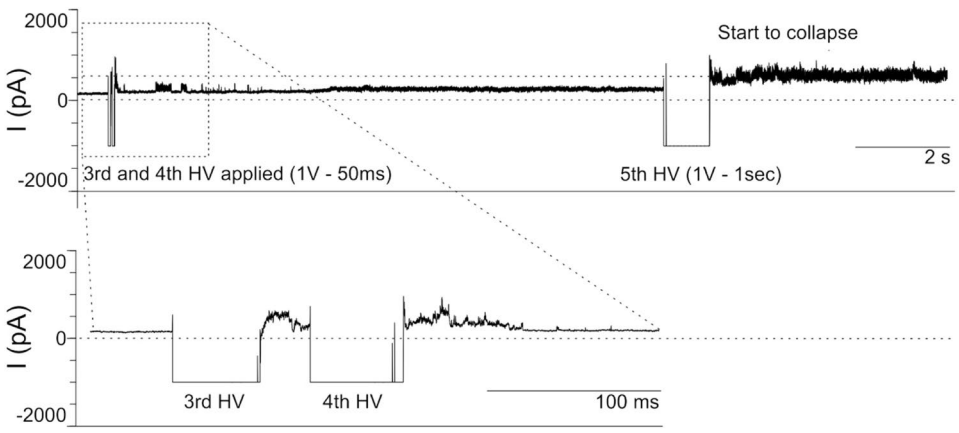

Fig. 4 Resealing characteristics of bilayer membrane when high voltage was applied. First two breakdowns show the 1 V and 50 ms long electrical field pulse. After the 5th high voltage (HV) application (1 V for 1 s), membrane disruption was observed. The data was taken at the end of the experiment, which continued for 33 h at 0 V. The graph at the bottom is an enlargement of the current–time trace recorded upon the application of the 3rd and 4th HV pulse

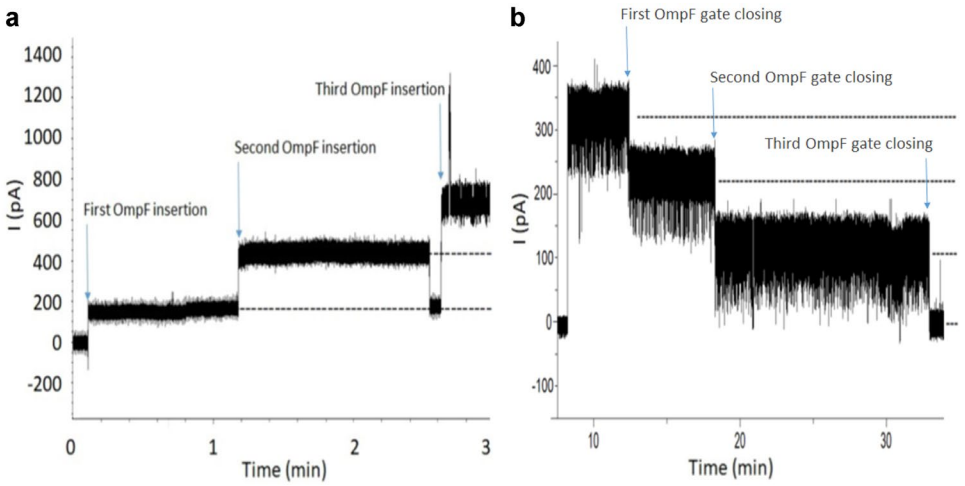

Fig. 5 Representative current–time traces for the OmpF porin insertion. A. Representative current–time trace showing successive insertion of 3 OmpF trimer at 200 mV (0.2 M KCl). B. Representative channel gating of one trimeric OmpF at 150 mV (0.5 M KCl). The sampling frequency was 50 kHz and the filtering frequency; 5 kHz)

single-channel characteristics of the OmpF porin. Each step-decrease in the recording indicates the channel gates that occur upon the application of the high voltage. This is very typical for OmpF porin which has a trimer structure; each monomer appears to gate upon the applications of voltages of 120 mV and above. Porin was usually inserted into the lipid membrane within 5 min. Immediately after the insertions were observed, the blockages due to the gate closures of OmpF were also observed with the applied voltage.

Conductance and radius of the porin can be connected by approximating the channel by a simple cylinder. Based on the current–time graph shown in Fig. 5a, the single channel conductance of OmpF trimer (0.2 M KCl) were obtained approximately 0.83 nS in agreement with literature. (Guzel and Citak 2018) It is reported in the literature that the internal loop L3 constricts the pore to an elliptical cross-section of 7×11 Å, at about half the height of the barrel (Cowan et al. 1992). Simple radius calculations of nanopores are calculated by following equation:

$$r = \sqrt{\frac{G \times l}{\pi \times \sigma}}$$

r: pore radius, G: Conductance, l: Porin length, σ: conductivity of electrolyte.

In our work, simple conductance calculations result in an equivalence constriction zone pore radius approximately 4 Å with corresponds to literature values (Zahn et al. 2016; Saint et al. 1996). These radius values were calculated by taking the average of five test results (See Supplementary Table 1).

4 Conclusion

In this study, we present a novel and cheap high voltage discharger set-up for the production of easy and controllable aperture openings on Teflon films to be used in multi and/or single-channel electrophysiology experiments. Our results show that Teflon films produced by our discharger possess good mechanical and physical performance comparable to those reported in the literature. The setting is straightforward to implement by any scientist working in the field. It is also an inexpensive alternative to the commercially available instruments widely used in the electrophysiology laboratories like high-frequency generators. We anticipate that the description for the development of a Teflon film driller using this high voltage discharger will benefit many in the field and can be further advanced by simple modifications to obtain smaller apertures for different purposes.

Supplementary Information The online version contains supplementary material available at https://doi.org/10.1007/s10544-021-00553-4.

Acknowledgements The authors would like to acknowledge funding from TUBITAK under grant number 117S114. The authors would also like to thank Halil Ibrahim Sag for useful discussions during the preliminary experiments.

Declarations

Disclosure statement No potential conflict of interest was reported by the authors.

References

G. Altamimi, H.A Illias, N. Mokhtar, H. Mokhlis, A.H.A Bakar, Corona discharges under various types of electrodes. IEEE International Conference on Power and Energy (PECon) IEEE, 5–8 (2014)

G. Bähr, A. Diederich, G. Vergères, M. Winterhalter, Interaction of the effector domain of MARCKS and MARCKS-related protein with lipid membranes revealed by electric potential measurements. Biochemistry **37**(46), 16252–16261 (1998)

Y.N.D. Bandara, B.I. Karawdeniya, J.R. Dwyer, Push-button method to create nanopores using a tesla-coil lighter. ACS omega **4**(1), 226–230 (2019)

R. Benz, K. Janko, W. Boos, P. Läuger, Formation of large, ion-permeable membrane channels by the matrix protein (porin) of Escherichia coli. Biochimica et Biophysica Acta (BBA)-Biomembranes **511**(3), 305–319 (1978)

A.L. Brown, B.E. Johnson, M.B. Goodman, Making patch-pipettes and sharp electrodes with a programmable puller. JoVE (Journal of Visualized Experiments), (20), p.e939 (2008)

S.W. Cowan, T. Schirmer, G. Rummel, M. Steiert, R. Ghosh, R.A. Pauptit, J.N. Jansonius, J.P. Rosenbusch, Crystal structures explain functional properties of two *E. coli* porins. Nature **358**(6389), 727–733 (1992)

T. Charitat, E. Bellet-Amalric, G. Fragneto, F. Graner, Adsorbed and free lipid bilayers at the solid-liquid interface. The European Physical Journal B-Condensed Matter and Complex Systems **8**(4), 583–593 (1999)

J.P. Dilger, R. Benz, Optical and electrical properties of thin monoolein lipid bilayers. The Journal of membrane biology **85**(2), 181–189 (1985)

M. Eray, N.S. Dogan, L. Liu, A.R. Koch, D.F. Moffett, M. Silber, B.J. Van Wie, Highly stable bilayer lipid membranes (BLMs) formed on microfabricated polyimide apertures. Biosens. Bioelectron. **9**(4–5), 343–351 (1994)

C.M. Gabe, S.J. Brookes, J. Kirkham, Preparative SDS PAGE as an alternative to His-Tag purification of recombinant amelogenin. Frontiers in physiology **8**, 424 (2017)

J.L. Gornall, K.R. Mahendran, O.J. Pambos, L.J. Steinbock, O. Otto, C. Chimerel, M. Winterhalter, U.F. Keyser, Simple reconstitution of protein pores in nano lipid bilayers. Nano Lett. **11**(8), 3334–3340 (2011)

T. Gutsmann, T. Heimburg, U. Keyser, K.R Mahendran, M. Winterhalter. Protein reconstitution into freestanding planar lipid membranes for electrophysiological characterization. nature protocols, **10**(1), 188 (2015)

F.D. Güzel, B. Miles, Development of in-flow label-free single molecule sensors using planar solid-state nanopore integrated microfluidic devices. Micro & Nano Letters **13**(9), 1352–1357 (2018)

F.D. Guzel, H. Avci, Fabrication of nanopores in an ultra-thin polyimide membrane for biomolecule sensing. IEEE Sens. J. **18**(7), 2641–2646 (2018)

F.D. Guzel, F. Citak, Development of an on-chip antibiotic permeability assay with single molecule detection capability. IEEE Trans. Nanobiosci. **17**(2), 155–160 (2018)

S.O. Hagge, H. de Cock, T. Gutsmann, F. Beckers, U. Seydel, A. Wiese, Pore formation and function of phosphoporin PhoE of Escherichia coli are determined by the core sugar moiety of lipopolysaccharide. J. Biol. Chem. **277**(37), 34247–34253 (2002)

S.O. Hagge, A. Wiese, U. Seydel, T. Gutsmann, Inner field compensation as a tool for the characterization of asymmetric membranes and peptide-membrane interactions. Biophys. J . **86**(2), 913–922 (2004)

W. Hanke, W.R. Schulue, Planar lipid bilayers: methods and applications. Academic Press (2012)

J.S. Hansen, M. Perry, J. Vogel, T. Vissing, C.R. Hansen, O. Geschke, J. Emnéus, C.H. Nielsen, Development of an automation technique for the establishment of functional lipid bilayer arrays. J. Micromech. Microeng. **19**(2), 025014 (2009)

T.A. Harroun, W.T. Heller, T.M. Weiss, L. Yang, H.W. Huang, Experimental evidence for hydrophobic matching and membrane-mediated interactions in lipid bilayers containing gramicidin. Biophys. J. **76**(2), 937–945 (1999)

O. Holst ed., Bacterial toxins: methods and protocols. Springer Science & Business Media **145** (2000)

K. Maex, M.R. Baklanov, D. Shamiryan, F. Lacopi, S.H. Brongersma, Z.S. Yanovitskaya, Low dielectric constant materials for microelectronics. J. Appl. Phys. **93**(11), 8793–8841 (2003)

G. Maglia, A.J. Heron, D. Stoddart, D. Japrung, H. Bayley, Analysis of single nucleic acid molecules with protein nanopores. In Methods in enzymology **475,** 591–623 Academic Press (2010)

T. Mahmood, P.C. Yang, Western blot: technique, theory, and trouble shooting. North American journal of medical sciences **4**(9), 429 (2012)

M. Mayer, J.K. Kriebel, M.T. Tosteson, G.M. Whitesides, Microfabricated teflon membranes for low-noise recordings of ion channels in planar lipid bilayers. Biophys. J . **85**(4), 2684–2695 (2003)

A. Molleman, Patch clamping: an introductory guide to patch clamp electrophysiology. John Wiley & Sons (2003)

B.N. Miles, A.P. Ivanov, K.A. Wilson, F. Doğan, D. Japrung, J.B. Edel, Single molecule sensing with solid-state nanopores: novel materials, methods, and applications. Chem. Soc. Rev. **42**(1), 15–28 (2013)

M. Montal, P. Mueller, Formation of bimolecular membranes from lipid monolayers and a study of their electrical properties. Proc. Natl. Acad. Sci. **69**(12), 3561–3566 (1972)

P. Mueller, D.O. Rudin, H.T. Tien, W.C. Wescott, Reconstitution of cell membrane structure in vitro and its transformation into an excitable system. Nature **194**(4832), 979–980 (1962)

A. Obergrussberger, S. Stölzle-Feix, N. Becker, A. Brüggemann, N. Fertig, C. Möller, Novel screening techniques for ion channel targeting drugs. Channels **9**(6), 367–375 (2015)

M.C. Peterman, J.M. Ziebarth, O. Braha, H. Bayley, H.A. Fishman, D.M. Bloom, Ion channels and lipid bilayer membranes under high potentials using microfabricated apertures. Biomed. Microdevice **4**(3), 231–236 (2002)

B.T. Priest, A.M. Swensen, O.B. McManus, Automated electrophysiology in drug discovery. Curr. Pharm. Des. **13**(23), 2325–2337 (2007)

N. Saint, K.L. Lou, C. Widmer, M. Luckey, T. Schirmer, J.P. Rosenbusch, Structural and functional characterization of OmpF porin mutants selected for larger pore size II. Functional characterization. J. Biol. Chem. **271**(34), 20676–20680 (1996)

M.E. Sandison, M. Zagnoni, M. Abu-Hantash, H. Morgan, Micromachined glass apertures for artificial lipid bilayer formation in a microfluidic system. J. Micromech. Microeng. **17**(7), S189 (2007)

M. Scanziani, M. Häusser, Electrophysiology in the age of light. Nature **461**(7266), 930–939 (2009)

C. Schmidt, M. Mayer, H. Vogel, A chip-based biosensor for the functional analysis of single ion channels. Angew. Chem. **112**(17), 3267–3270 (2000)

C.G. Siontorou, G.P. Nikoleli, D.P. Nikolelis, S.K. Karapetis, Artificial lipid membranes: past, present, and future. Membranes **7**(3), 38 (2017)

P.U. SiamratPhonkaphon, Influences of Relative Humidity on the Electric Field and Potential on Suspension Insulator String. Energy Procedia **89**, 110–119 (2016)

A.D. Stokes, W.T. Oppenlander, Electric arcs in open air. J. Phys. D Appl. Phys. **24**(1), 26 (1991)

X. Wang, D. Teng, Q. Guan, R. Mao, Y. Hao, X. Wang, J. Yao, J. Wang, Escherichia coli outer membrane protein F (OmpF): an immunogenic protein induces cross-reactive antibodies against Escherichia coli and Shigella. AMB Express **7**(1), 155 (2017)

S.J. Wilk, L. Petrossian, M. Goryll, T.J. Thornton, S.M. Goodnick, J.M. Tang, R.S. Eisenberg, Integrated electrodes on a silicon based ion channel measurement platform. Biosens. Bioelectron. **23**(2), 183–190 (2007)

M. Winterhalter, Lipid membranes in external electric fields: kinetics of large pore formation causing rupture. Adv. Coll. Interface. Sci. **208**, 121–128 (2014)

W.F. Wonderlin, A.F.R.J. Finkel, R.J. French, Optimizing planar lipid bilayer single-channel recordings for high resolution with rapid voltage steps. Biophys. J . **58**(2), 289–297 (1990)

S.P. Wrenn, E. Small, N. Dan, Bubble nucleation in lipid bilayers: A mechanism for low frequency ultrasound disruption. Biochimica et Biophysica Acta (BBA)-Biomembranes, **1828**(4), 1192–1197 (2013)

M. Zahn, S.P. Bhamidimarri, A. Baslé, M. Winterhalter, B. Van den Berg, Structural insights into outer membrane permeability of Acinetobacter baumannii. Structure **24**(2), 221–231 (2016)

D. Zhang, Patch Clamp: A Powerful technique for studying the mechanism of acupuncture. Evidence-Based Complementary and Alternative Medicine (2012)

S. Zhu, C. Gong, L. Ren, X. Li, D. Song, G. Zheng, A simple and effective strategy for solving the problem of inclusion bodies in recombinant protein technology: His-tag deletions enhance soluble expression. Appl. Microbiol. Biotechnol. **97**(2), 837–845 (2013)